Divalent Ion-Specific Outcomes on Stern Layer Structure and Total Surface Potential at the Silica:Water Interface

Emily Ma and Franz M. Geiger*

Department of Chemistry, Northwestern University, 2145 Sheridan Road, Evanston, Illinois 60660, United States

ABSTRACT. The second-order nonlinear susceptibility, $\chi^{(2)}$, in the Stern layer, and the total interfacial potential drop, $\Phi(0)_{tot}$, across the oxide:water interface are estimated from SHG amplitude and phase measurements for divalent cations (Mg^{2+}, Ca^{2+}, Sr^{2+}, Ba^{2+}) at the silica:water interface at pH 5.8 and various ionic strengths. We find that interfacial structure and total potential depend strongly on ion valency. We observe statistically significant differences between the experimentally determined $\chi^{(2)}$ value for NaCl and that of the alkali earth series, but smaller differences between ions of the same valency in that series. These differences are particularly pronounced at intermediate salt concentrations, which we attribute to the influence of hydration structure in the Stern layer. Furthermore, we corroborate the differences by examining the effects of anion substitution (SO_4^{2-} for Cl^-). Finally, we identify that hysteresis in measuring the reversibility of ion adsorption and desorption at fused silica in forward and reverse titrations manifests itself both in Stern layer structure and in total interfacial potential for some of the salts, most notable $CaCl_2$ and $MgSO_4$, but less so for $BaCl_2$ and NaCl.

*Corresponding author: f-geiger@northwestern.edu

I. Introduction. Ion specific interactions at charged interfaces have been explored intensely over the years[1-4] but they are challenging to incorporate into models. At mineral/oxide interfaces, mobile ions form an electrical double layer (EDL) that extends from the solid surface into the aqueous bulk, modulating electrostatic interactions and balancing the charges that exist at the interface. Longstanding questions remain about what molecular properties govern EDL structure.[5-7] Descriptions of charged interfaces have been commonly based on empirical models such as the Hofmeister series or mean-field theory.[8, 9] While these models are adequate for a description of macroscopic behavior, they do not provide a proper fundamental molecular level description of interactions within the EDL, nor a chemical understanding of interfacial electrostatics.[7, 9] As a specific example, primitive ion models treat all alkali earth cations as having the same +2 charge, neglecting important ion-specific properties such as hydration environment or hardness/softness.

Over the years, much work has sought to fill in those necessary aspects and to provide a detailed description of both hydration structure of ions[5] and its influence on the electrostatic potential at an interface.[10] An important question that has arisen from such studies concerns whether electrolyte valency (z) is a reasonable description of ion correlations at the interface as well as the overall potential that exists at an aqueous interface. Another question that has arisen pertains to the interplay between molecular interactions and electrostatics at the interface. Our previous work has examined these types of questions in the context of monovalent ions and their effects on hydration structure at the silica/water interface.[11] Exploring these questions with divalent ions offers an opportunity to pursue fundamental investigations of ion specific EDL structure and electrostatics at aqueous interfaces.

Alkali earth cations are common in the environment, play a large role in a variety of geochemical processes and are often not only associated with chloride but also the sulfate counter

ion, which is one of the most earth abundant inorganic anions.[1, 2, 12, 13] Second-order nonlinear spectroscopies[14-17] provide an appealing perspective for building a comprehensive molecular description of divalent cations at charged aqueous/solid interfaces.[18] These methods can be carried out in real time, at ambient temperature and pressure, under aqueous flow conditions, and are generally nondestructive to the sample. We now employ a recently developed new variant of this method, namely heterodyne-second harmonic generation (HD-SHG), which provides the SHG amplitude and phase.[11, 19-23] Both parameters yield point estimates of two important interfacial electrostatic and structural parameters, namely the total surface potential ($\Phi(0)_{tot}$) and the second order nonlinear susceptibility, $\chi^{(2)}$. We obtain these two parameters for the alkali earth cation series Mg^{2+}, Ca^{2+}, Sr^{2+}, and Ba^{2+} and evaluate differences among each ion at a given concentration between the μM and 100 mM range at pH 5.8, as well as between the various species. The $\chi^{(2)}$ and $\Phi(0)_{tot}$ point estimates for the alkali earth cations are smaller in magnitude than the ones obtained for NaCl. We find that $\chi^{(2)}$ is essentially invariant for the alkali earth chlorides but that their point estimates for $\Phi(0)_{tot}$ decrease with increasing cation radius. We also find anionic-specific effects in $\chi^{(2)}$ upon substituting chloride for sulfate. We discuss these outcomes in the context of changes in interfacial hydration structure reported from atomistic simulations. Finally, under our experimental conditions, hysteresis is observed in $\chi^{(2)}$ and $\Phi(0)_{tot}$ when increasing vs. decreasing the analyte concentration for calcium and barium chloride as well as magnesium sulfate.

II. Methods.

A. Sample and Solution Preparation. Details of our liquid flow cell have been described previsouly.[11, 19-22] Silica hemispheres (Hyperion Optics, Corning 7979 IR-grade) were cleaned as previously described using an Alnochromix (Alconox) sulfuric acid cleaning solution.[11, 20, 21] We obtained NaCl from Sigma-Aldrich (Part # 746398, Lot # SLBK2618V, ≥99% pure), Na_2SO_4

from Fisher Scientific (Anhydrous, Catalog # S421-500, ≥99% pure), $MgCl_2$ $6H_2O$ from Sigma Aldrich (Part # 499609, ≥99% pure), $CaCl_2$ $2H_2O$ from Sigma-Aldrich (Part # 21115, ≥99% pure), $SrCl_2$ from Acros Organics (Catalog # 369740050, 99.9%), and $BaCl_2$ from Mallinckrodt (99.9%). Stock solutions were prepared for all salts using ultrapure water (Millipore-Sigma 18.2MΩ) at 1M ionic strength. The solutions were diluted further to the various concentrations and left exposed to laboratory air overnight to reach equilibrium with atmospheric CO_2 (pH 5.7 $\pm$0.2) prior to usage in the experiments to avoid formation of any hydroxides with the divalent cation species in solution[24] or complexation on silica substrate in the form of hydrates.[25, 26] No further filtration was carried out prior to experimentation.

B. Experiments. Details of our HD-SHG spectrometer have been previously described.[11, 19-22] Solutions were flowed through a home-built Teflon sample cell at a rate of 5 mL min^{-1} for ten minutes for a complete exchange of the sample cell contents. This process was monitored using homodyne-detected SHG. We have previously found the sample cell exchange time to be around three to four minutes.[19] Interference fringes were collected by translating an α-quartz crystal 30 equidistant positions along a 100 mm translational stage, with an acquisition time of approximately 3 minutes per fringe. Sets of five replicate interference fringes were collected for each ionic strength/salt concentration condition, over a period of 20 minutes. We control for phase drift by clamping in the sample cell two to three hours prior to the experiment, after which the spectrometer's phase is stable for up to six hours.[21]

The salt titrations were performed in a stepwise fashion, with five replicate measurements acquired for each aqueous phase condition. Each salt titration was repeated once, and our analysis is from the duplicate isotherms. Starting at ultrapure water (Millipore-Sigma 18.2MΩ cm, pH 5.8, 2 μM ionic strength), we increase the ionic strength in steps of factors of ten until the highest ionic

strength of 100 mM, after which we return the ionic strength in a stepwise fashion to the starting condition of ultrapure water at 2 μM. Using the procedure described, the phase drift during the duration of the experiment is negligible (<1°).

C. Data Fitting, Phase Referencing Procedure, and Point Estimates of Φ_0 and $\chi^{(2)}$. We utilize our previously published methods to extract the parameters needed for calculating the second order nonlinear susceptibility and surface potential. The generated interference patterns are fit to a sinusoidal function:

$$y = y_0 + Acos(fx + \varphi_{fit}) \quad (1)$$

Here, y_0 is the signal intensity offset, the SHG amplitude, A, corresponds to the SHG signal, E_{sig}, f is the periodicity of our spectrometer, x is the position on the translational stage, and the SHG phase, φ_{sig}, is obtained from φ_{fit}. Both A and φ_{fit} are obtained by fitting eqn. 1 to the SHG interference fringes. The φ_{fit} obtained at 2 μM pH 5.7 is set to $60^o \pm 1^o$, which is the previously determined phase difference between that ionic solution condition and the one obtained for 500 mM NaCl at pH 2.5,[20] the measured point of zero charge (PZC) of silica,[1, 2, 27, 28] where the Coulombic contribution to the total interfacial potential is zero. The SHG phase, φ_{sig}, at 2 μM and pH 5.7 is then $+60^o \pm 1^o$.

The non-resonant SHG amplitude and phase obtained from eqn. 1 yields the total second-order nonlinear susceptibility in our HD-SHG spectrometer according to:[20]

$$E_{sig} \times e^{i\varphi_{sig}} \propto \chi^{(2)}_{tot} = \chi^{(2)} - \Phi(0)_{tot}\chi^{(3)}_{water}\left[\cos\left(\varphi_{DC,EDL}\right) e^{i\varphi_{DC,EDL}} + 1.5i\right] \quad (2)$$

Here, $\chi^{(2)}$ is the second-order nonlinear susceptibility of the interface, which is given by the sum of the second-order nonlinear susceptibilities of the interfacial species (in order of abundance, these are interfacial water molecules, then the surface silanol groups, and then the anions and cations adsorbed to the protonated and deprotonated surface silanol groups, respectively, *vide*

infra). The third-order contribution in eqn. 2 is multiplied into the total interfacial potential, $\Phi(0)_{tot}$, which includes all electrostatic contributions (Coulomb, dipole, and multipolar potentials, *vide infra*). The third-order term is dominated by the third-order contribution from the water molecules in the EDL, which is given by $\chi^{(3)}_{water}$ ($9.6 \pm 1.9 \times 10^{-22}$ m^2V^{-2} from off-resonant SHG experiments at the air/water interface or 10.3×10^{-22} m^2V^{-2} estimated from the third-order molecular hyperpolarizability obtained through quantum mechanical calculations).[29, 30] The third-order response from the water molecules in the EDL is modulated by the phase, $\varphi_{DC,EDL}$, associated with the electrostatic DC field emanating from the charged interface into the bulk. For an exponentially decaying field, the DC phase angle is given by $\varphi_{DC,EDL} = atan(\Delta k_z \lambda_D)$, where Δk_z is the wavevector mismatch and λ_D the Debye screening length at a given bulk ionic strength, computed from Debye Hückel theory. For our experimental geometry, Δk_z is 1.1 x 10^7 m^{-1}. The Debye length for each of our experimental conditions of ionic strength is determined using Debye-Hückel theory using bulk water's relative permittivity of 78. We recently reported[20] an additional purely imaginary third-order contribution that may be of quadrupolar nature, $i\chi^{(3)}_X$, where, $\chi^{(3)}_X \approx 1.5 \times \chi^{(3)}_{water}$.

Dipole and multipolar contributions are included in measurements of the differential capacitance of electrolyte:oxide:semiconductor devices,[28, 31, 32] as well as XPS signals from silica colloidal jets.[33-35] Both methods produce pH-dependent total interfacial potentials for the silica:water interface at various [salt] that agree well with our recently published HD-SHG-derived total potentials.[20] We therefore conclude that measurements of the SHG amplitude and phase provide the total interfacial potential drop across the oxide:water interface. It contains the Coulomb, dipole, quadrupole, and all other contributions, $\Phi(0)_i$, to the interfacial potential drop,[36]

and is quantified from the measured SHG amplitude, E_{sig}, and phase, φ_{sig}, for a given DC phase angle, φ_{DC}, according to[19, 20]

$$\Phi(0)_{tot} = \sum_i \Phi(0)_i = -\frac{C}{R} \times \frac{E_{sig} \sin(\varphi_{sig})}{\chi^{(3)}_{water}\{cos(\varphi_{DC}) \sin(\varphi_{DC}) + 1.5\}} \quad (3)$$

For silica substrates, the C/R ratio is $3.6 \times 10^{-22} m^2 V^{-1}$ in our spectrometer.[20]

Interfacial water is an ideal species to probe with nonlinear optics. Even though the non-resonant 2nd-order hyperpolarizability of water, $a^{(2)}$, is modest,[37] it is by far the majority species in most aqueous interfacial systems and often aligned in the Stern layer. How an array of water molecules is aligned in the Stern layer is encoded in the second-order susceptibility, a fundamental structural property of matter in noncentrosymmetric environments.[15] It is a measure of how the electrons are distributed in a non-centrosymmetric medium (the interface) and given by the number *Ni* of a given interfacial species *i* multiplied by the orientational average of the hyperpolarizability, $\alpha_i^{(2)}$.[17, 38, 39] HD-SHG quantifies $\chi^{(2)}$ from the measured SHG amplitude and phase according to[19, 20]

$$\chi^{(2)} = \sum_i N_i \langle \alpha_i^{(2)} \rangle = \frac{C}{R} \times \left(E_{sig}\right) \cos\left(\varphi_{sig}\right) + \Phi(0)_{tot}\, \chi^{(3)}_{water} \cos^2(\varphi_{DC}) \quad (4),$$

employing the $\Phi(0)_{tot}$ from eqn. 3 and the same C/R ratio.

III. Results and Discussion.

A. SHG Amplitudes and Phases. Figures 1A and B show the SHG amplitude and the SHG phase for the range of NaCl, $MgCl_2$, $CaCl_2$, $SrCl_2$, and $BaCl_2$ concentrations indicated. Our earlier homodyne-detected SHG measurements indicate that the cation surface coverage increases with increasing cation concentration[40-42] up to an estimated saturation level of approximately 10^{12} ions per square cm. This coverage corresponds to the number of negatively charged adsorption sites (SiO^- groups) on silica at circumneutral pH reported from XPS measurements.[43]

Our current HD-SHG measurements reveal a nonmonotonic trend in the recorded SHG amplitude for the aqueous NaCl solution, as recently reported.[11, 19] In contrast, the divalent chloride salts show a less pronounced, weakly non-monotonic trend with increasing ionic strength in the SHG amplitude.

In our previous work,[21] we determined a phase shift ($\Delta\varphi_{sig}$) of $29.7 \pm 0.7°$ for the pristine fused silica/water interface for hemispheres that were first exposed to ultrapure water (2 μM) at pH 5.7 ± 0.1 and then to 100 mM NaCl at the same pH. Here, we observe the same result, as well as similar overall φ_{sig} values for $MgCl_2$, and $SrCl_2$, as shown in Fig. 1B. However, we observe a larger SHG phase shift for $BaCl_2$ and $CaCl_2$ ($\Delta\varphi_{sig,BaCl2} = 36^o$ and $\varphi_{sig,CaCl2} = 25^o$) in comparison to NaCl, $MgCl_2$, and $SrCl_2$. We observe similar behavior in the SHG amplitude and phase when comparing Na_2SO_4 and $MgSO_4$ with their respective chloride salts (Fig. 1C and D). The SHG amplitude (Fig. 1C) is similar for both sulfate salts regardless of the cation identity. The SHG phase shifts relative to pure water (Figure 1D) across both sulfate and chloride species are approximately 30^o for all four salts surveyed.

B. Estimated Trends in $\Phi(0)_{tot}$ and $\chi^{(2)}$ Across the Cations. Our recent report shows a possible method of separating the second- and third-order contributions to the SHG signal and therefore estimating interfacial structure and potential using eqn. 2,[20] resulting in eqns. 3 and 4. We now use this method to determine how the second order nonlinear susceptibility ($\chi^{(2)}$) and the total surface potential, $\Phi(0)_{tot}$, depend on the chemical identity of the adsorbed ions and their concentrations. Fig. 2A shows a large difference in $\chi^{(2)}$ between NaCl and all the divalent cations, but no statistically significant difference in the $\chi^{(2)}$ values among the divalent chloride salts. Fig. 2B reveals differences in $\chi^{(2)}$ when sulfate is introduced as an anion (for both Na and the Mg salts). The $\Phi(0)_{tot}$ point estimates reveal a statistically significantly larger difference among the alkali

earth chlorides we surveyed (bottom halves of Fig. 2). These differences do not follow the ionic radius of each cation species, which matches findings from previous work, including from calorimetric measurements.[44-46] Ca^{2+} appears to have the largest field screening effect in the cation series, with $\Phi(0)_{tot}$ reaching close to 0 V at 100 mM ionic strength. The larger ions, strontium and barium, come next, while the smallest (and hardest) ion, magnesium, lowers $\Phi(0)_{tot}$ the least relative to NaCl.

Eqn. 4 shows that $\chi^{(2)}$ is a linear combination of the contributions from the individual interfacial constituents.[21, 23] These are, in our case, the interfacial water molecules, then the surface silanol groups, and then the anions and cations adsorbed to the protonated and deprotonated surface silanol groups, respectively. The $\chi^{(2)}$ value from the interfacial water and surface silanol groups should be close to the one obtained at the lowest ionic strength (ultrapure water, 2 μM ionic strength, pH 5.8) condition. We therefore subtract this $\chi^{(2)}$ value from the data shown in Fig. 2 and obtain, at least to leading order, the $\chi^{(2)}$ values of the ions bound to the interfacial SiO^- and $SiOH_2^+$ sites (Fig. 3). The results indicate non-monotonic behavior and a maximum in $\chi^{(2)}$ around 0.1 mM ionic strength for most of the salts we surveyed. We also find a change in the sign of $\chi^{(2)}$ at an ionic strength around 1 mM for the divalent chloride salts we studied (Fig. 3A), and to a lesser extent in the sulfates (Fig. 3B). This observation would be expected in case of a flip in the net orientation of the radiating dipoles that produce the SHG response based on trends documented in previous studies.[47-49] We therefore find experimental evidence for a significant change in interfacial structure with increasing surface coverage for some of the ions we surveyed, consistent with reports by others for mica:water[50-53] and silica:water[47-49, 54] interfaces. Previous studies of divalent cations, specifically magnesium and calcium, by Gibbs and co-workers,[55, 56] have shown that low concentrations of these salts (0.033mM) attenuate the vibrational sum frequency generation

(SFG)-resonant water signal in comparison to NaCl at similar concentrations albeit at a higher pH than the conditions studied here. The resonant vibrational SFG experiments attributed these trends to displacement of the hydration layer above the silica surface by ions retaining their centrosymmetric hydration shell.[55] These trends were attributed to close association of Ca^{2+} to the interface,[55, 57-62] a finding that would be consistent with the non-resonant $\chi^{(2)}$ estimates reported here (as well as the largest reduction in interfacial potential by $CaCl_2$ relative to NaCl).

These results are in some ways surprising. Previous studies that have explored hydration structure and the point of zero charge of silica indicate that cation identity has an outsize effect on the electrostatics over structure at the interface.[63] Likewise, previous x-ray reflectivity studies have revealed that hydration shell structures play a role in trends of interfacial potential.[34, 63-65] However, understanding the effects of different multivalent cations on surface charge density remains a point of contention. Potentiometric titrations by Dove and Craven[45] have shown reverse lyotropic effects on surface charge density at the silica/water interface, in the order $SrCl_2 < BaCl_2 < CaCl_2 < MgCl_2$. Furthermore, calorimetric titrations by the Kabengi group have also shown slower uptake of M^{2+} ions at the interface relative to M^+ ions with a positive lyotropic effect on heats of adsorption for increasing ionic radius.[44] In these experiments, the observed trends in ΔH_{ads} were strongly correlated with hydration properties for the monovalent ions, but did not hold as strongly for the divalent cations. Adsorption phenomena and changes in that behavior for various alkali earth cations were instead attributed to bare ionic radius and ionic potential (or charge/radius ratio).[44] Our findings may corroborate this scenario given differences between cation species in our experiments decrease with increasing surface coverage. Studies of the muscovite/water interface have also demonstrated that divalent ions with larger electron density such as Sr^{2+} can adsorb in both fully and partially hydrated states.[52, 66] Different adsorption mechanisms for counterion

species with larger electron may explain the larger magnitude surface potential for Sr^{2+} and Ba^{2+} at 100mM, in spite of similar $\chi^{(2)}$ values in comparison to Ca^{2+} and Mg^{2+} at higher surface coverages.

With the observed trends in $\chi^{(2)}$ among all divalent ions, we compare our findings to previous studies that have examined the effects of increasing ion size on the overall hyperpolarizability in different molecular systems. From our experimental measurements, we find relatively small changes in the second order nonlinear susceptibility between the divalent halide salts. This outcome is surprising given the precedent for relatively large changes in the hydration structure at the interface.[45, 55] Simulations have shown, for example, a highly ordered first solvation shell for divalent cations such as Mg^{2+} vs a fairly labile hydration structure for Na^{+}.[67] Furthermore, Na^{+} is predicted to form direct contact ion pairs with silanol groups, whereas Mg^{2+} is proposed to not bind directly to silanol groups at the surface, but rather form a hydrogen bonded complex through its tightly bonded hydration sphere.[67] Other MD simulations have shown $Ca(OH)^{+}$ can form at the silica surface upon deprotonation of one of the water molecules in the hydration shell of the Ca^{2+} cation.[68] Previous theoretical studies of model complexes have indicated that hyperpolarizabilities generally increase with ionic radius,[69, 70] but our experiments show little changes between ions to such extent. These studies have also found a threefold increase in the hyperpolarizability in these complexes between substitution of Ca^{2+} with Na^{+}. However, when examining the normalized $\chi^{(2)}$ values, Ca^{2+} and Mg^{2+} represent the smallest change in comparison to Na^{+} observed in these experiments.[68] These are also the hardest cations in the series we studied.

C. Chloride vs Sulfate. We applied the same analysis to anion identity to corroborate whether cation behavior did indeed play the largest role at the interface. While positively charged counterions make up most of the species in the Stern layer under the conditions explored in our

experiments (pH 5.8), previous experiments have shown a small number of $SiOH^+$ groups present even at neutral pH conditions.[71] In titrations of Na_2SO_4 and $MgSO_4$, we observe changes in both and Φ_0 (Fig. 2B) and $\chi^{(2)}$ (Fig. 3B) indicating that the presence of sulfate anions may have outsize effects on interactions at the interface, where the establish the largest negative potential at ionic strengths < 1mM.[72, 73] Sulfates have been postulated to lead to silica dissolution through salting out effects that become especially pronounced at high temperatures.[26] In spite of silica's overall negative charge at circumneutral pH,[45, 71] we observe a reduction in $\chi^{(2)}$ and Φ_0 with the addition of Na_2SO_4 which demonstrates that the anion species likely plays a role in the electrical double layer[72] even though the "standard" electrical double layer model (e.g. Gouy-Chapman-Stern theory) predicts Na^+ should be the predominant surface-bound species.[47, 74, 75] We observe the opposite trend for the 2:2 salt $MgSO_4$ which could indicate that sulfate ions have a notable influence on the magnesium ion coverage. We postulate that these may play a role in the changes in overall structure that facilitate salting out effects (i.e. sulfate-silicic acid structures that form) at higher concentrations.[26] We also note that the Φ_0 point estimates for chloride and sulfate anions are invariant between each shared cation species at ionic strengths > 1 mM, which may indicate little change to hydration structure in the diffuse layer at higher concentrations.

D. Hysteresis and Manifestation in Φ_0 and $\chi^{(2)}$. Another aspect we explore in this study is the dependence of adsorption and desorption reversibility on the cation identity. We perform reverse salt titrations immediately after the forward titration, reducing the salt concentration in a stepwise fashion using the same procedures as the forward titration. The preservation of the timescales from the previous stepwise titration is chosen to determine whether we arrive at the same structural and electrostatic parameters under the same ionic strength conditions and experimental time scale

(approximately three hours per forward titration and the equivalent amount of time for the reverse titration).

Among all salts studied (Fig. 4 and S8-12) we observe the largest difference in $\chi^{(2)}$ values for $CaCl_2$ (Fig. 4A), for which the $\chi^{(2)}$ point estimates are ~1.5 times larger in magnitude for the reverse titration in the lower concentration regime. The magnitude of the potential, on the other hand, is smaller for the reverse titration, again in the lower concentration regime. We observe these effects are less pronounced for $BaCl_2$ and $SrCl_2$ (Fig. 4A and S10). The $MgSO_4$ reversibility manifests itself largely in the surface potential (Fig. 4C), while NaCl shows only very minor differences in interfacial structure and surface potential (Fig. 4D). Taken together, we find clear ion-specific outcomes on the structural and electrostatic hysteresis of our system for several of the salts we studied.

These results can be viewed in light of previous studies that have shown hysteresis in mineral oxide systems depends strongly on water structure as well as surface charge density.[46] Previous calculations of energies of adsorption indicate Ca^{2+} likely forms a tighter contact ion pair with the silica surface disrupting the hydration structure at the surface than ions with a larger hydration shell, such as Ba^{2+}.[54] These findings may demonstrate why larger hysteretic effects present for the $CaCl_2$ salts compared to the other divalent cations. Surprisingly, we observe the least amount of hysteresis when using NaCl, at least under our present experimental conditions. A previous study we performed on a faster timescale, where the salt concentration was immediately jumped from ultrapure water to 100mM NaCl and vice versa, however, did demonstrate path-dependent effects.[19] The differences between these two outcomes highlight the importance of characterizing each step in surface-specific experiments involving fused silica, water, and salts.

Conclusions and Outlook. Divalent cations at the silica/water interface probed with non-resonant HD-SHG spectroscopy measurements reveal that interfacial structure and total potential depend strongly on ion valency. When purely evaluating cation identity, we observe significant differences between the experimentally determined $\chi^{(2)}$ value for NaCl and alkali earth cations, but smaller differences between ions of the same valency in that series. These differences are amplified at intermediate salt concentrations, which we attribute to the influence of hydration structure in the Stern layer, which is the origin of $\chi^{(2)}$. Furthermore, we corroborate the differences we report by examining the effects of anion substitution. Finally, we identify that hysteresis in measuring the reversibility of ion adsorption and desorption at fused silica under the stated conditions of our experiments manifests itself both in Stern layer structure, $\chi^{(2)}$, and in total interfacial potential, $\Phi(0)_{tot}$.

Our estimates of $\chi^{(2)}$ are directly comparable to atomistic simulations of interfacial structure at aqueous interfaces that readily produce the second-order nonlinear susceptibility for resonant[76-82] and non-resonant conditions.[19, 75] While adding the resonant $\chi^{(2)}$ values to the $\chi^{3)}\Phi(0)_{tot}$ contribution (eqn. 2) through a simultaneous HD-SHG/HD-SFG experiment has not yet been achieved, the non-resonant $\chi^{(2)}$ values reported here are obtained directly through eqn. 4 and comparison to atomistic simulations is possible: the first approach calculating $\chi^{(2)}$ values for a charged interface (oxide:salt solution) was pioneered in 2019 by Chen and Singer,[75] focusing on the polarization of the water molecules. This method was recently expanded by us and the Miller group[19] to include surface hydroxyl groups, the second-most abundant interfacial species besides water at oxide:water interfaces. While that approach distinguished contact ion pairs from solvent-separated ion pairs and showed the presence of the former recapitulated the experimentally observed trends in $\chi^{(2)}$, ion specific effects were not pursued in that study.

Our $\chi^{(2)}$ estimates should be similarly informative for identifying those structural arrangements in the production runs of atomistic simulations that recapitulate the experimental $\chi^{(2)}$ values at oxide:water interfaces at a given pH (or surface charge), ion identity, and ionic strength. Likewise, we expect that the estimates of the $\Phi(0)_{tot}$ drop across the oxide:water interface we report here for the various salts we surveyed provides an experimental benchmark for mean field and/or atomistic models that include dipolar and multipolar contributions to the popular Gouy-Chapman-Stern theory,[83] the "standard model". Ionizing surface potential measurements published in 2021 by Allen and coworkers show that the surface potential ("χ potential",[84] no relation to $\chi^{(2)}$ reported here) of the (nominally uncharged) pure air:water interface is as low as ~ –500 mV,[85] and that it is slightly less negative (~ -400 mV) at the air:electrolyte (1 M NaCl and 1M Na_2SO_4) interface. Dipolar arrays of interfacial water molecules are thought to be the main contributors to this potential.[86-88] Multipolar contributions may also be important.[85, 89-91] Our own work with the Miller group[19] and the preceding study by Chen and Singer[75] also show surface potentials due to water polarization at negatively charged oxide:electrolyte interfaces estimated from molecular dynamics simulations are negative and in the range of multiple tens of mV, decreasing in magnitude with ionic strength. Those outcomes are consistent with earlier MD reports on structured water at charged aqueous:insulator interfaces, by, for instance, Borguet and Klein and co-workers.[92] New mean-field models beyond the standard model have been introduced that account for non-ideal behavior (short-range ion correlations, surface site availability, etc.) of aqueous electrolytes and ionic liquids.[93-97] A related issue is the spatial variation of the (field-dependent) relative permittivity, ε_r, which the standard model neglects, i.e. the solvent is modeled as a uniform continuum, despite large differences in reported ε_r.[97-105] The experimentally determined $\Phi(0)_{tot}$ estimates obtained here include all the contributions to the potential and should thus be an

appropriate experimental benchmark to which theory must conform. It will also be informative to determine how ion-specific effects manifests themselves on other oxides, such as hematite,[106, 107] which is an area we are actively pursuing.

V. Associated Content

Supporting Information: optical fringe data, $\chi^{(2)}$ and $\Phi(0)_{tot}$ point estimates for forward and reverse titrations, for all salts studied.

Acknowledgement. We gratefully acknowledge support from Northwestern University.

References

1. Langmuir, D., *Aqueous Environmental Chemistry*. Prentice Hall: Upper Saddle River, NJ 1997.

2. Lyklema, J., *Fundamentals of Interface and Colloid Science*. Elsevier: 2000.

3. Brown, G. E.; Parks, G. A., Sorption of trace elements on mineral surfaces: Modern perspectives from spectroscopic studies, and comments on sorption in the marine environment. *Int. Geo. Rev.* **2001,** *43*, 963-1073.

4. Brown, G. E., How Minerals React with Water. *Science* **2001,** *294* (5540), 67-70.

5. Ben-Amotz, D.; Underwood, R., Unraveling Water's Entropic Mysteries: A Unified View of Nonpolar, Polar, and Ionic Hydration. *Accounts of Chemical Research* **2008,** *41* (8), 957-967.

6. Jungwirth, P., Hofmeister Series of Ions: A Simple Theory of a Not So Simple Reality. *The Journal of Physical Chemistry Letters* **2013,** *4* (24), 4258-4259.

7. Jungwirth, P.; Cremer, P. S., Beyond Hofmeister. *Nature Chemistry* **2014,** *6* (4), 261-263.

8. Stirnemann, G.; Wernersson, E.; Jungwirth, P.; Laage, D., Mechanisms of Acceleration and Retardation of Water Dynamics by Ions. *J. Am. Chem. Soc.* **2013,** *135*, 11824.

9. Jungwirth, P.; Tobias, D. J., Specific Ion Effects at the Air/Water Interface. *Chem. Rev.* **2006,** *106*, 1259-1281.

10. Gmür, T. A.; Goel, A.; Brown, M. A., Quantifying Specific Ion Effects on the Surface Potential and Charge Density at Silica Nanoparticle–Aqueous Electrolyte Interfaces. *The Journal of Physical Chemistry C* **2016,** *120* (30), 16617-16625.

11. Boamah, M. D.; Ohno, P. E.; Lozier, E.; Van Ardenne, J.; Geiger, F. M., Specifics about Specific Ion Adsorption from Heterodyne-Detected Second Harmonic Generation. *J. Phys. Chem. B* **2019,** *123*, 5848-56.

12. Faure, G., *Principles and Applications of Geochemistry*. 2nd ed.; Prentice Hall: New Jersey, 1998.

13. Evangelou, V. P., *Environmental Soil and Water Chemistry*. John Wiley & Sons: New York, 1998.

14. Boyd, R. W., *Nonlinear Optics*. Academic Press: New York, 1992.

15. Mukamel, S., *Principles of Nonlinear Optical Spectroscopy*. Oxford University Press: Oxford, 1995.

16. Shen, Y. R., *The Principles of Nonlinear Optics*. John Wiley & Sons, Inc.: Hoboken, NJ, 2003.

17. Morita, A., *Theory of Sum Frequency Generation Spectroscopy*. Springer: 2018; Vol. 97.

18. Geiger, F. M., Second Harmonic Generation, Sum Frequency Generation, and $\chi(3)$: Dissecting Environmental Interfaces with a Nonlinear Optical Swiss Army Knife. *Annual Review of Physical Chemistry* **2009,** *60* (1), 61-83.

19. Ma, E.; Kim, J.; Chang, H.; Ohno, P. E.; Jodts, R. J.; Miller III, T. F.; Geiger, F. M., Stern and Diffuse Layer Interactions during Ionic Strength Cycling. *J. Phys. Chem. C* **2021,** *125*, 18002-14.

20. Ma, E.; Ohno, P. E.; Kim, K.; Liu, Y.; Lozier, E. H.; Miller III, T. F.; Wang, H.-f.; Geiger, F. M., A New Imaginary Term in the 2nd Order Nonlinear Susceptibility from Charged Interfaces. *J. Phys. Chem. Lett.* **2021,** *12* (24), 5649-59.

21. Ohno, P. E.; Chang, H.; Spencer, A. P.; Liu, Y.; Boamah, M. D.; Wang, H.-f.; Geiger, F. M., Beyond the Gouy–Chapman Model with Heterodyne-Detected Second Harmonic Generation. *The Journal of Physical Chemistry Letters* **2019,** *10* (10), 2328-2334.

22. Chang, H.; Ohno, P. E.; Liu, L.; Geiger, F. M., Direct Measurement of Charge Reversal on Lipid Bilayers using Heterodyne-Detected Second Harmonic Generation Spectroscopy. *chemRxiv.8678450.v1* **2019**.

23. Ohno, P. E.; Chang, H.; Spencer, A. P.; Liu, Y.; Boamah, M. D.; Wang, H.-f.; Geiger, F. M., Correction to Beyond the Gouy-Chapman Model with Heterodyne-Detected Second Harmonic Generation. *J. Phys. Chem. Lett.* **2019,** *10*, 5364.

24. Müller, B. *ChemEQL*, 3.0; Limnological Research Center, Swiss Federal Institute of Aquatic Science and Technology: Kastanienbaum, Switzerland, 2005.

25. Greenberg, S. A., REACTION BETWEEN SILICA AND CALCIUM HYDROXIDE SOLUTIONS. I. KINETICS IN THE TEMPERATURE RANGE 30 TO 85°1. *The Journal of Physical Chemistry* **1961,** *65* (1), 12-16.

26. House, W. A., The Role of Surface Complexation in the Dissolution Kinetics of Silica: Effects of Monovalent and Divalent Ions at 25°C. *Journal of Colloid and Interface Science* **1994,** *163* (2), 379-390.

27. Stumm, W.; Morgan, J. J., *Aquatic Chemistry*. John Wiley & Sons, Inc.: New York, 1996; Vol. 3rd ed.

28. Bousse, L.; De Rooij, N. F.; Bergveld, P., Operation of Chemically Sensitive Field-Effect Sensors As a Function of the Insulator-Electrolyte Interface. *IEEE Trans. Electron Devices* **1983,** *ED-30*, 1263-70.

29. Dalstein, L.; Chiang, K.-Y.; Wen, Y.-C., Direct Quantification of Water Surface Charge by Phase-Sensitive Second Harmonic Spectroscopy. *The Journal of Physical Chemistry Letters* **2019,** *10* (17), 5200-5205.

30. Lütgebaucks, C.; Gonella, G.; Roke, S., Optical label-free and model-free probe of the surface potential of nanoscale and microscopic objects in aqueous solution. *Phys. Rev. B* **2016,** *94* (19), 195410.

31. Bousse, L., Single electrode potentials related to flat-band voltage measurements on EOS and MOS structures. *J. Chem. Phys.* **1982,** *76*, 5128-33.

32. Diot, J. L.; Joseph, J.; Martin, J. R.; Clechet, P., pH Dependence of the Si/SiO2 Interface State Density for EOS Systems: Quasi-Static and AC Conductance Methods. *J. Electroanal. Chem.* **1985,** *193*, 75-88.

33. Brown, M. A.; Abbas, Z.; Kleibert, A.; Green, R. G.; Goel, A.; May, S.; Squires, T. M., Determination of Surface Potential and Electrical Double-Layer Structure at the Aqueous Electrolyte-Nanoparticle Interface. *Phys. Rev. X* **2016,** *6*, 011007.

34. Brown, M. A.; Bossa, G. V.; May, S., Emergence of a Stern Layer from the Incorporation of Hydration Interactions into the Gouy–Chapman Model of the Electrical Double Layer. *Langmuir* **2015,** *31*, 11477-11483.

35. Brown, M. A.; Goel, A.; Abbas, Z., Effect of Electrolyte Concentration on the Stern Layer Thickness at a Charged Interface. *Angewandte Chemie International Edition* **2016,** *55* (11), 3790-3794.

36. Chang, H.; Ohno, P. E.; Liu, L.; Geiger, F. M., Direct Measurement of Charge Reversal on Lipid Bilayers using Heterodyne-Detected Second Harmonic Generation Spectroscopy. *J. Phys. Chem. B* **2020,** *124* (641-9).

37. Le Breton, G.; Bonhomme, O.; Brevet, P.-F.; Benichou, E.; Loison, C., Hyperpolarizability of Water at the Air-Vapor Interface: Numerical Modeling Questions Standard Experimental Approximations. *chemRxiv 10.26434/chemrxiv.14216837.v1* **2021**.

38. Boyd, R. W., *Nonlinear Optics, 3rd Edition*. Elsevier Academic Press Inc: San Diego, 2008; p 1-613.

39. Shen, Y. R., *The Principles of Nonlinear Optics*. John Wiley & Sons: New York, 1984.

40. Hayes, P. L.; Malin, J. N.; Konek, C. T.; Geiger, F. M., Interaction of Nitrate, Barium, Strontium and Cadmium Ions with Fused Quartz/Water Interfaces Studied by Second Harmonic Generation *J. Phys. Chem. A* **2008,** *112*, 660-668.

41. Malin, J. N.; Hayes, P. L.; Geiger, F. M., Interactions of Ca, Zn, and Cd Ions at Buried Solid/Water Interfaces Studied by Second Harmonic Generation†. *The Journal of Physical Chemistry C* **2008,** *113* (6), 2041-2052.

42. Malin, J. N.; Hayes, P. L.; Geiger, F. M., Interactions of Ca, Zn, and Cd Ions at Buried Solid/Water Interfaces Studied by Second Harmonic Generation. *J. Phys. Chem. C* **2009,** *113* (6), 2041.

43. Duval, Y.; Mielczarski, J. A.; Pokrovsky, O. S.; Mielczarski, E.; Ehrhardt, J. J., Evidence of the Existence of Three Types of Species at the Quartz-Aqueous Solution Interface at pH 0-10: XPS Surface Group Quantification and Surface Complexation Modeling. *J. Phys. Chem. B.* **2002,** *106* (11), 2937-2945.

44. Allen, N.; Machesky, M. L.; Wesolowski, D. J.; Kabengi, N., Calorimetric Study of Alkali and Alkaline-Earth Cation Adsorption and Exchange at the Quartz-Solution Interface. *J. Colloid Interface Sci.* **2017,** *504*, 538.

45. Dove, P. M.; Craven, C. M., Surface Charge Density on Silica in Alkali and Alkaline Earth Chloride Electrolyte Solutions. *Geochim. Cosmochim. Acta* **2005,** *69*, 4963.

46. Karlsson, M.; Craven, C.; Dove, P. M.; Casey, W. H. J. A. G., Surface Charge Concentrations on Silica in Different 1.0 M Metal-Chloride Background Electrolytes and Implications for Dissolution Rates. **2001,** *7* (1), 13-32.

47. Marchioro, A.; Bischoff, M.; Lütgebaucks, C.; Biriukov, D.; Předota, M.; Roke, S., Surface Characterization of Colloidal Silica Nanoparticles by Second Harmonic Scattering: Quantifying the Surface Potential and Interfacial Water Order. *The Journal of Physical Chemistry C* **2019,** *123* (33), 20393-20404.

48. Jena, K. C.; Covert, P. A.; Hore, D. K., The Effect of Salt on the Water Structure at a Charged Solid Surface: Differentiating Second- and Third-order Nonlinear Contributions. *The Journal of Physical Chemistry Letters* **2011,** *2* (9), 1056-1061.

49. Ahmed, M.; Nihonyanagi, S.; Kundu, A.; Yamaguchi, S.; Tahara, T., Resolving the Controversy over Dipole versus Quadrupole Mechanism of Bend Vibration of Water in Vibrational Sum Frequency Generation Spectra. *The Journal of Physical Chemistry Letters* **2020,** *11* (21), 9123-9130.

50. Brugman, S. J. T.; Werkhoven, B. L.; Townsend, E. R.; Accordini, P.; van Roij, R.; Vlieg, E., Monovalent – divalent cation competition at the muscovite mica surface: Experiment and theory. *Journal of Colloid and Interface Science* **2020,** *559*, 291-303.

51. Adapa, S.; Malani, A., Role of hydration energy and co-ions association on monovalent and divalent cations adsorption at mica-aqueous interface. *Scientific Reports* **2018,** *8* (1), 12198.

52. Park, C.; Fenter, P. A.; Nagy, K. L.; Sturchio, N. C., Hydration and distribution of ions at the mica-water interface. *Physical Review Letters* **2006,** *97* (1).

53. Kobayashi, K.; Liang, Y.; Murata, S.; Matsuoka, T.; Takahashi, S.; Nishi, N.; Sakka, T., Ion Distribution and Hydration Structure in the Stern Layer on Muscovite Surface. *Langmuir* **2017,** *33* (15), 3892-3899.

54. Leung, K.; Criscenti, L. J.; Knight, A. W.; Ilgen, A. G.; Ho, T. A.; Greathouse, J. A., Concerted Metal Cation Desorption and Proton Transfer on Deprotonated Silica Surfaces. *J. Phys. Chem. Lett.* **2018,** *9*, 5379.

55. Rashwan, M.; Rehl, B.; Sthoer, A.; Darlington, A. M.; Azam, M. S.; Zeng, H.; Liu, Q.; Tyrode, E.; Gibbs, J. M., Structure of the Silica/Divalent Electrolyte Interface: Molecular Insight into Charge Inversion with Increasing pH. *The Journal of Physical Chemistry C* **2020,** *124* (49), 26973-26981.

56. Darlington, A. M.; Jarisz, T. A.; Dewalt-Kerian, E. L.; Roy, S.; Kim, S.; Azam, M. S.; Hore, D. K.; Gibbs, J. M., Separating the pH-Dependent Behavior of Water in the Stern and Diffuse Layers with Varying Salt Concentration. *The Journal of Physical Chemistry C* **2017**.

57. Raji, F.; Ejtemaei, M.; Nguyen, A. V., Resolving the mystery of the second charge reversal on solid surfaces in the presence of divalent heavy metal ions. *Applied Surface Science* **2020,** *529*, 147128.

58. Piontek, S. M.; Tuladhar, A.; Marshall, T.; Borguet, E., Monovalent and Divalent Cations at the α-Al2O3(0001)/Water Interface: How Cation Identity Affects Interfacial Ordering and Vibrational Dynamics. *J. Phys. Chem. C* **2019,** *123*, 18315.

59. Porus, M.; Labbez, C.; Maroni, P.; Borkovec, M., Adsorption of Monovalent and Divalent Cations on Planar Water-Silica Interfaces Studied by Optical Reflectivity and Monte Carlo Simulations. *J. Chem. Phys.* **2011,** *135*, 064701.

60. Hu, X.; Li, Y.; Sun, H.; Song, X.; Li, Q.; Cao, X.; Li, Z., Effect of Divalent Cationic Ions on the Adsorption Behavior of Zwitterionic Surfactant at Silica/Solution Interface. *The Journal of Physical Chemistry B* **2010,** *114* (27), 8910-8916.

61. Parsons, D. F.; Ninham, B. W., Charge Reversal of Surfaces in Divalent Electrolytes: The Role of Ionic Dispersion Interactions. *Langmuir* **2010,** *26*, 6430.

62. Lorenz, C. D.; Travesset, A., Charge Inversion of Divalent Ionic Solutions in Silica Channels. *Phys. Rev. E: Stat., Nonlinear, Soft Matter Phys.* **2007,** *75*, 061202.

63. Brown, M. A.; Goel, A.; Abbas, Z., Effect of Electrolyte Concentration on the Stern Layer Thickness at a Charged Interface. *Angew. Chem., Int. Ed.* **2016,** *55*, 3790.

64. Brown, M. A.; Abbas, Z.; Kleibert, A.; Green, R. G.; Goel, A.; May, S.; Squires, T. M., Determination of Surface Potential and Electrical Double-Layer Structure at the Aqueous Electrolyte-Nanoparticle Interface. *Physical Review X* **2016,** *6* (1), 011007.

65. Brown, M. A.; Beloqui Redondo, A.; Sterrer, M.; Winter, B.; Pacchioni, G.; Abbas, Z.; van Bokhoven, J. A., Measure of Surface Potential at the Aqueous–Oxide Nanoparticle Interface by Xps from a Liquid Microjet. *Nano Lett.* **2013,** *13*, 5403.

66. Hayes, P. L.; Malin, J. N.; Konek, C. T.; Geiger, F. M., Interaction of Nitrate, Barium, Strontium and Cadmium Ions with Fused Quartz/Water Interfaces Studied by Second Harmonic Generation. *The Journal of Physical Chemistry A* **2008,** *112* (4), 660-668.

67. Lowe, B. M.; Skylaris, C. K.; Green, N. G.; Shibuta, Y.; Sakata, T., Calculation of Surface Potentials at the Silica–Water Interface Using Molecular Dynamics: Challenges and Opportunities. *Japanese journal of applied physics* **2018,** *57*, 04FM02.

68. Wang, X.; Liu, W.; Duan, H.; Wang, B.; Han, C.; Wei, D., The Adsorption Mechanism of Calcium Ion on Quartz (101) Surface: A DFT Study. *Powder Technol.* **2018,** *329*, 158.

69. Arif, A. M.; Yousaf, A.; Xu, H.-l.; Su, Z.-M., N-(O-methoxyphenyl)aza-15-crown-5-ether derivatives: Highly efficient and wide range nonlinear optical response based cation recognition. *Journal of Molecular Liquids* **2020,** *301*, 112492.

70. Hatua, K.; Mondal, A.; Banerjee, P.; Nandi, P. K., Diffuse electron of alkali metals (Li, Na, K) or diffuse electron pair of alkaline earth metals (Be, Mg, Ca) which predict larger second hyperpolarizability? A comprehensive study of M···NH3 model compounds. *Chemical Physics Letters* **2018,** *692*, 160-165.

71. Duval, Y.; Mielczarski, J. A.; Pokrovsky, O. S.; Mielczarski, E.; Ehrhardt, J. J., Evidence of the Existence of Three Types of Species at the Quartz−Aqueous Solution Interface at pH 0−10: XPS Surface Group Quantification and Surface Complexation Modeling. *The Journal of Physical Chemistry B* **2002,** *106* (11), 2937-2945.

72. Hua, W.; Jubb, A. M.; Allen, H. C., Electric Field Reversal of Na2SO4, (NH4)2SO4, and Na2CO3 Relative to CaCl2 and NaCl at the Air/Aqueous Interface Revealed by Heterodyne Detected Phase-Sensitive Sum Frequency. *J. Phys. Chem. Lett.* **2011,** *2*, 2515.

73. Jubb, A. M.; Allen, H. C., Sulfate Adsorption at the Buried Fluorite–Solution Interface Revealed by Vibrational Sum Frequency Generation Spectroscopy. *The Journal of Physical Chemistry C* **2012,** *116* (16), 9085-9091.

74. Pezzotti, S.; Galimberti, D. R.; Shen, Y. R.; Gaigeot, M.-P., Structural definition of the BIL and DL: a new universal methodology to rationalize non-linear chi(2) SFG signals at charged interfaces, including chi(3) contributions. *Physical Chemistry Chemical Physics* **2018,** *20* (7), 5190-5199.

75. Chen, S.-H.; Singer, S., Molecular Dynamics Study of the Electric Double Layer and Nonlinear Spectroscopy at the Amorphous Silica- Water Interface. *J. Phys. Chem. A* **2019,** *123*, 6364-84.

76. Morita, A.; Hynes, J. T., A Theoretical Analysis of the Sum Frequency Generation Spectrum of the Water Surface. II. Time-Dependent Approach. *J. Phys. Chem. B* **2002,** *106*, 673-685.

77. Zhang, Y.; de Aguiar, H. B.; Hynes, J. T.; Laage, D., Water Structure, Dynamics, and Sum-Frequency Generation Spectra at Electrified Graphene Interfaces. *J. Phys. Chem. Lett.* **2020,** *11*, 624-31.

78. Cyran, J. D.; Donovan, M. A.; Vollmer, D.; Brigiano, F. S.; Pezzotti, S.; Galimberti, D. R.; Gaigeot, M.-P.; Bonn, M.; Backus, E. H., Molecular hydrophobicity at a macroscopically hydrophilic surface. *Proc. Natl. Acad. Sci. U S A* **2019,** *116*, 1520-5.

79. Pezzotti, S.; Galimberti, D. R.; Shen, Y. R.; Gaigeot, M.-P., Structural definition of the BIL and DL: a new universal methodology to rationalize non-linear χ(2)(ω) SFG signals at charged interfaces, including χ(3)(ω) contributions. *Physical Chemistry Chemical Physics* **2018,** *20* (7), 5190-5199.

80. Pezzotti, S.; Galimberti, D.; Shen, Y.; Gaigeot, M.-P., What the Diffuse Layer (DL) Reveals in Non-Linear SFG Spectroscopy. *Minerals* **2018,** *8* (7), 305.

81. Pezzotti, S.; Galimberti, D. R.; Gaigeot, M.-P., 2D H-Bond Network as the Topmost Skin to the Air–Water Interface. *J. Phys. Chem. Lett.* **2017,** *8*, 3133-3141.

82. Reddy, S. K.; Thiraux, R.; Wellen Rudd, B. A.; Lin, L.; Adel, T.; Joutsuka, T.; Geiger, F. M.; Allen, H. C.; Morita, A.; Paesani, F., Bulk Contributions Modulate the Sum-Frequency Generation Spectra of Water on Model Sea-Spray Aerosols. *Chem* **2018,** *4*, 1629-44.

83. Stern, O., Zur Theorie der Elektrolytischen Doppelschicht. *Z. Elektrochem.* **1924,** *30*, 508-16.

84. Trasatti, S., Relative and Absolute Electrochemical Quantities. *J. Chem. Soc. Faraday Trans. 1* **1974,** *70*, 1752-68.

85. Adel, T.; Velez-Alvarez, J.; Co, A. C.; Allen, H., C., Circuit Analysis of Ionizing Surface Potential Measurements of Electrolyte Solutions. *J. Electrochem. Soc.* **2021,** *168*, 016507.

86. Casper, C. B.; Verreault, D.; Adams, E. M.; Hua, W.; Allen, H. C., Surface Potential of DPPC Monolayers on Concentrated Aqueous Salt Solutions. *Journal of Physical Chemistry B* **2016,** *120* (8), 2043-2052.

87. Bonthuis, D. J.; Horinek, D.; Bocquet, L.; Netz, R. R., Electrohydraulic Power Conversion in Planar Nanochannels. *Phys. Rev. Lett.* **2009,** *103*, 144503.

88. Rodriguez, D.; Marquez, M. D.; Zenasni, O.; Han, L. T.; Baldelli, S.; Lee, R. T., Surface Dipoles Induce Uniform Orientation in Contacting Polar Liquids. *Chem. Mat.* **2020,** *32*, 7832-41.

89. Doyle, C. C.; Shi, Y.; Beck, T. L., The Importance of the Water Molecular Quadrupole for Estimating Interfacial Potential Shifts Acting on Ions Near the Liquid−Vapor Interface. *J. Phys. Chem. B* **2019,** *123*, 3348-58.

90. Cendagorta, J. R.; Ichiye, T., The Surface Potential of the Water-Vapor Interface from Classical Simulations. *J. Phys. Chem. B* **2015,** *119*, 9114-9122.

91. Leung, K., Surface Potential at the Air-Water Interface Computed Using Density Functional Theory. *J. Phys. Chem. Lett.* **2010,** *1*, 496-9.

92. Dewan, S.; Carnevale, V.; Bankura, A.; Eftekhari-Bafrooei, A.; Fiorin, G.; Klein, M. L.; Borguet, E., Structure of Water at Charged Interfaces: A Molecular Dynamics Study. *Langmuir* **2014,** *30*, 8056-65.

93. Bazant, M. Z.; Kilic, M. S.; Storey, B. D.; Ajdari, A., Towards an understanding of induced-charge electrokinetics at large applied voltages in concentrated solutions. *J. Coll. Int. Sci.* **2009,** *152*, 48-88.

94. Fedorov, M. V.; Kornyshev, A. A., Ionic liquids at electried interfaces. *Chem. Rev.* **2014,** *114*, 2978-3036.

95. Goodwin, Z. A., .; Feng, G.; Kornyshev, A. A., Mean-Field Theory of Electrical Double Layer In Ionic Liquids with Account of Short- Range Correlations. *Electrochimica Acta* **2017,** *225*, 190-7.

96. Goodwin, Z. A., .; Kornyshev, A. A., Underscreening, Over- screening and Double-Layer Capacitance. *Electrochem. Comm.* **2017,** *82*, 129-33.

97. Pilon, L.; Wang, H.; d''Entremont, A., Recent Advances in Continuum Modeling of Interfacial and Transport Phenomena in Electric Double Layer Capacitors. *J. Electrochem. Soc.* **2015,** *162*, A5158-78.

98. Boamah, M. D.; Ohno, P. E.; Geiger, F. M.; Eisenthal, K. B., Relative Permittivity in the Electrical Double Layer from Nonlinear Optics. *J. Chem. Phys.* **2018,** *148*, 222808.

99. Kurosaki, S., The Dielectric Behavior of Sorbed Water on Silica Gel. *The Journal of Physical Chemistry* **1954,** *58* (4), 320-324.

100. Sakamoto, T.; Nakamura, H.; Uedaira, H.; Wada, A., High-frequency dielectric relaxation of water bound to hydrophilic silica gels. *The Journal of Physical Chemistry* **1989,** *93* (1), 357-366.

101. Wander, M. C. F.; Clark, A. E., Structural and Dielectric Properties of Quartz−Water Interfaces. *The Journal of Physical Chemistry C* **2008,** *112* (50), 19986-19994.

102. Schlaich, A.; Knapp, E. W.; Netz, R. R., Water Dielectric Effects in Planar Confinement. *Physical Review Letters* **2016,** *117* (4), 048001.

103. Sahai, N.; Sverjensky, D. A., Evaluation of internally consistent parameters for the triple-layer model by the systematic analysis of oxide surface titration data. *Geochimica Et Cosmochimica Acta* **1997,** *61* (14), 2801-2826.

104. Teschke, O.; Ceotto, G.; de Souza, E. F., Interfacial water dielectric-permittivity-profile measurements using atomic force microscopy. *Physical Review E* **2001,** *64* (1), 011605.

105. Fumagalli, L., et al., Anomalously low dielectric constant of confined water. *Science* **2018,** *360*, 1339-42.

106. Troiano, J. M.; Jordan, D. S.; Hull, C. J.; Geiger, F. A., Interaction of Cr(III) and Cr(VI) with Hematite Studied by Second Harmonic Generation. *J. Phys. Chem. C* **2013,** *117*, 5146-5171.

107. Jordan, D. S.; Hull, C. J.; Troiano, J. M.; Riha, S. C.; Martinson, A. B. F.; Rosso, K. M.; Geiger, F. M., Second Harmonic Generation Studies of Fe(II) Interactions with Hematite (alpha-Fe2O3). *Journal of Physical Chemistry C* **2013,** *117* (8), 4040-4047.

Figure Captions:

Figure 1. SHG amplitude A) and C) and phase B) and D) recorded for NaCl (dark green), $MgCl_2$, $CaCl_2$, $SrCl_2$, and $BaCl_2$ (light to dark blue), and Na_2SO_4 (orange), $MgCl_2$ (blue), and $MgSO_4$ (red), all at the ionic strengths indicated, and pH 5.8. Standard deviation between replicate measurements indicated by colored shading between point estimates.

Figure 2: Point estimates for $\chi^{(2)}$ (top half) and total surface potential (bottom half) for A) NaCl (dark green), $MgCl_2$, $CaCl_2$, $SrCl_2$, $BaCl_2$ (light to dark blue) and B) NaCl (dark green), Na_2SO_4 (orange), $MgCl_2$ (blue), and $MgSO_4$ (red), all at the ionic strengths indicated, and pH 5.8. Standard deviation between replicate measurements indicated by colored shading between point estimates.

Figure 3: Point estimates for $\chi^{(2)}$ for A) NaCl (dark green), $MgCl_2$, $CaCl_2$, $SrCl_2$, $BaCl_2$ (light to dark blue) and B) for NaCl (dark green), Na_2SO_4 (orange), $MgCl_2$ (blue), and $MgSO_4$ (red), all at the ionic strengths indicated, and pH 5.8. Standard deviation between replicate measurements indicated by colored shading between point estimates.

Figure 4: Point estimates for $\chi^{(2)}$ (top half) and $\Phi(0)$ (bottom half) from forward and reverse titrations, indicated by arrows, for A) $CaCl_2$, B) $BaCl_2$, C), $MgSO_4$, and D) NaCl, all at the ionic strengths indicated, and pH 5.8. Standard deviation between replicate measurements indicated by colored shading between point estimates.

Figure 1:

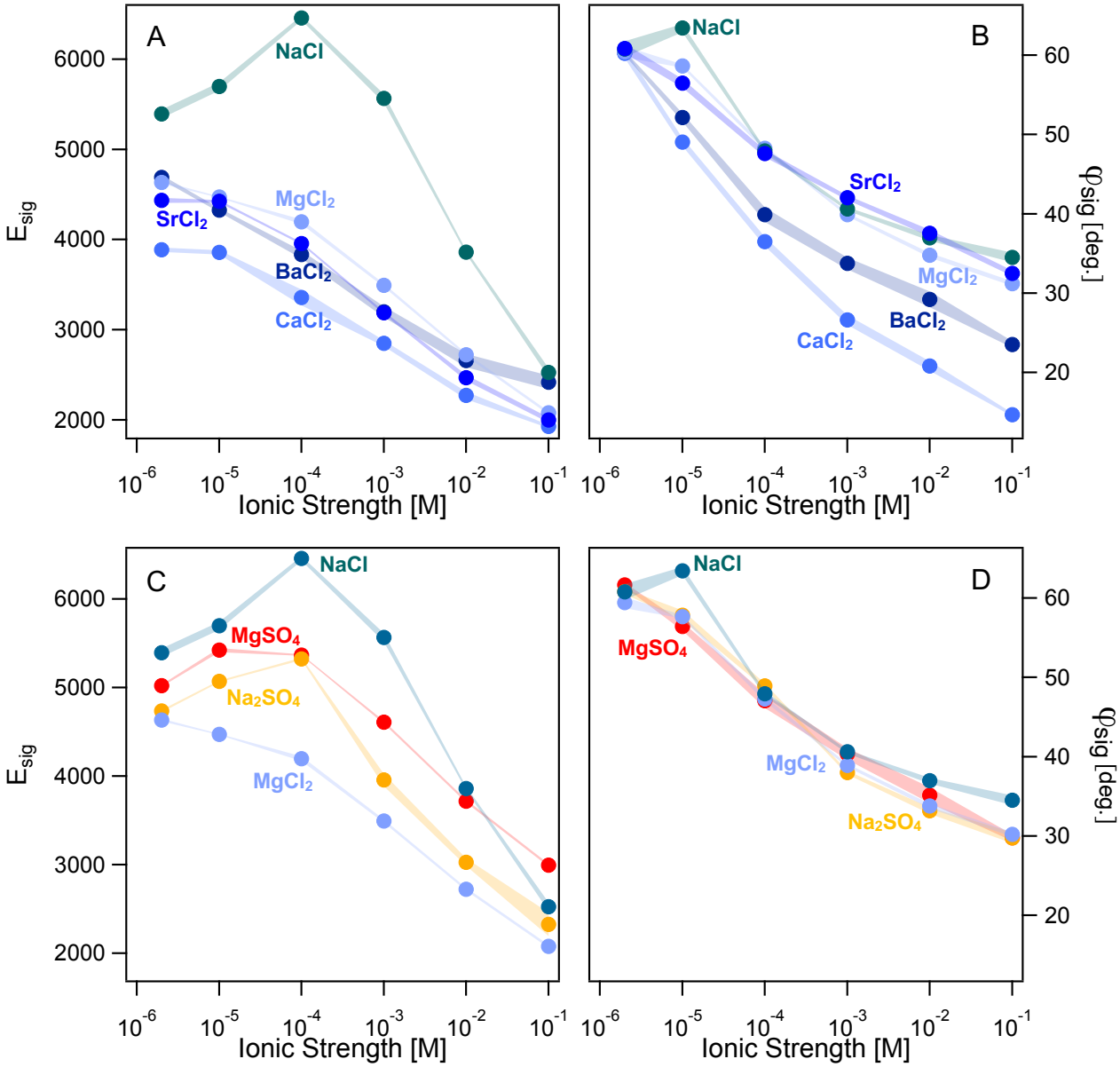
A
B
C
D
NaCl
MgCl2
SrCl2
BaCl2
CaCl2
MgSO4
Na2SO4
Esig
φsig [deg.]
Ionic Strength [M]
6000
5000
4000
3000
2000
60
50
40
30
20
10-6
10-5
10-4
10-3
10-2
10-1

Figure 2:

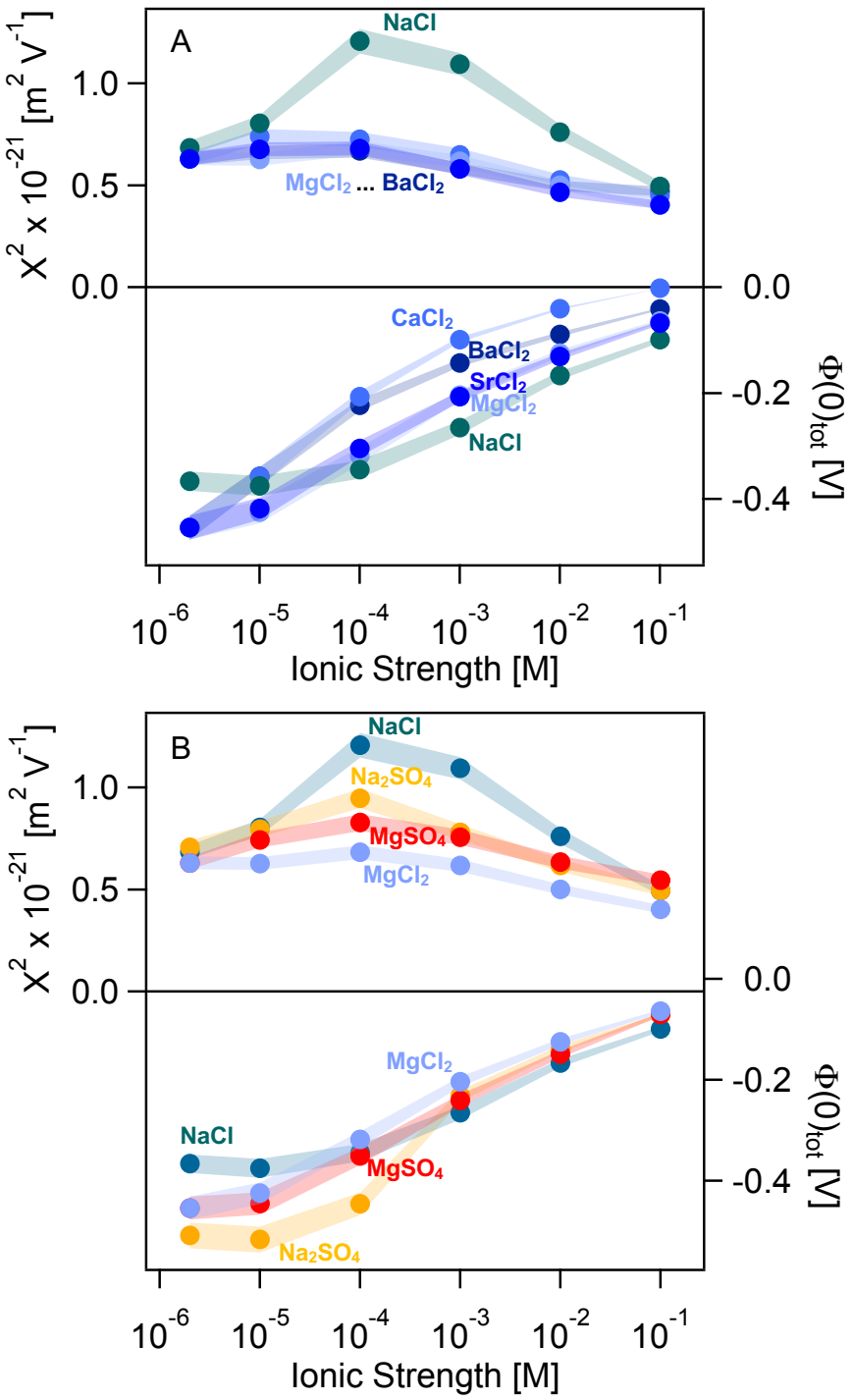
A
NaCl
MgCl2 ... BaCl2
CaCl2
BaCl2
SrCl2
MgCl2
NaCl
X2 x 10-21 [m2 V-1]
Φ(0)tot [V]
Ionic Strength [M]
B
NaCl
Na2SO4
MgSO4
MgCl2
NaCl
MgSO4
Na2SO4
X2 x 10-21 [m2 V-1]
Φ(0)tot [V]
Ionic Strength [M]

Figure 3:

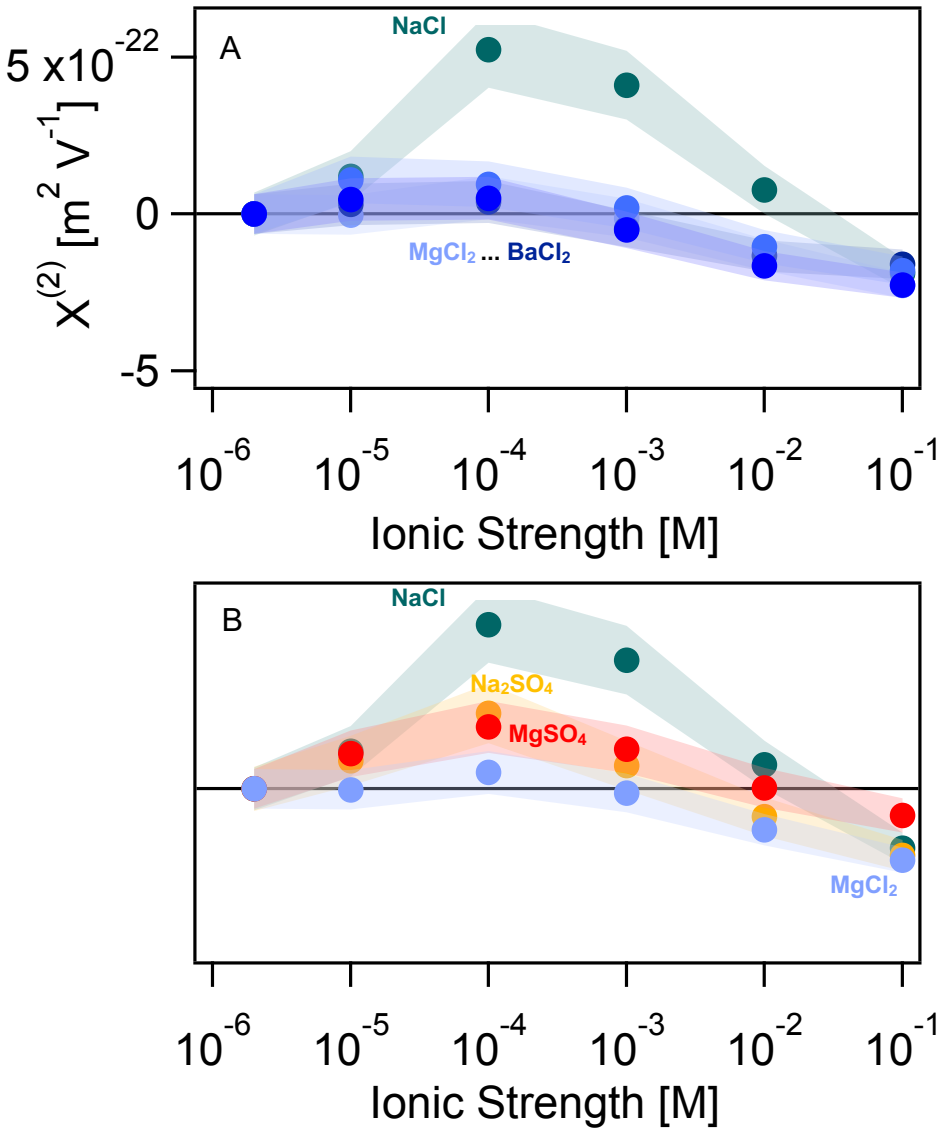
A
NaCl
MgCl2 ... BaCl2
5 x10-22
0
-5
χ(2) [m2 V-1]
10-6
10-5
10-4
10-3
10-2
10-1
Ionic Strength [M]
B
NaCl
Na2SO4
MgSO4
MgCl2
10-6
10-5
10-4
10-3
10-2
10-1
Ionic Strength [M]

Figure 4:

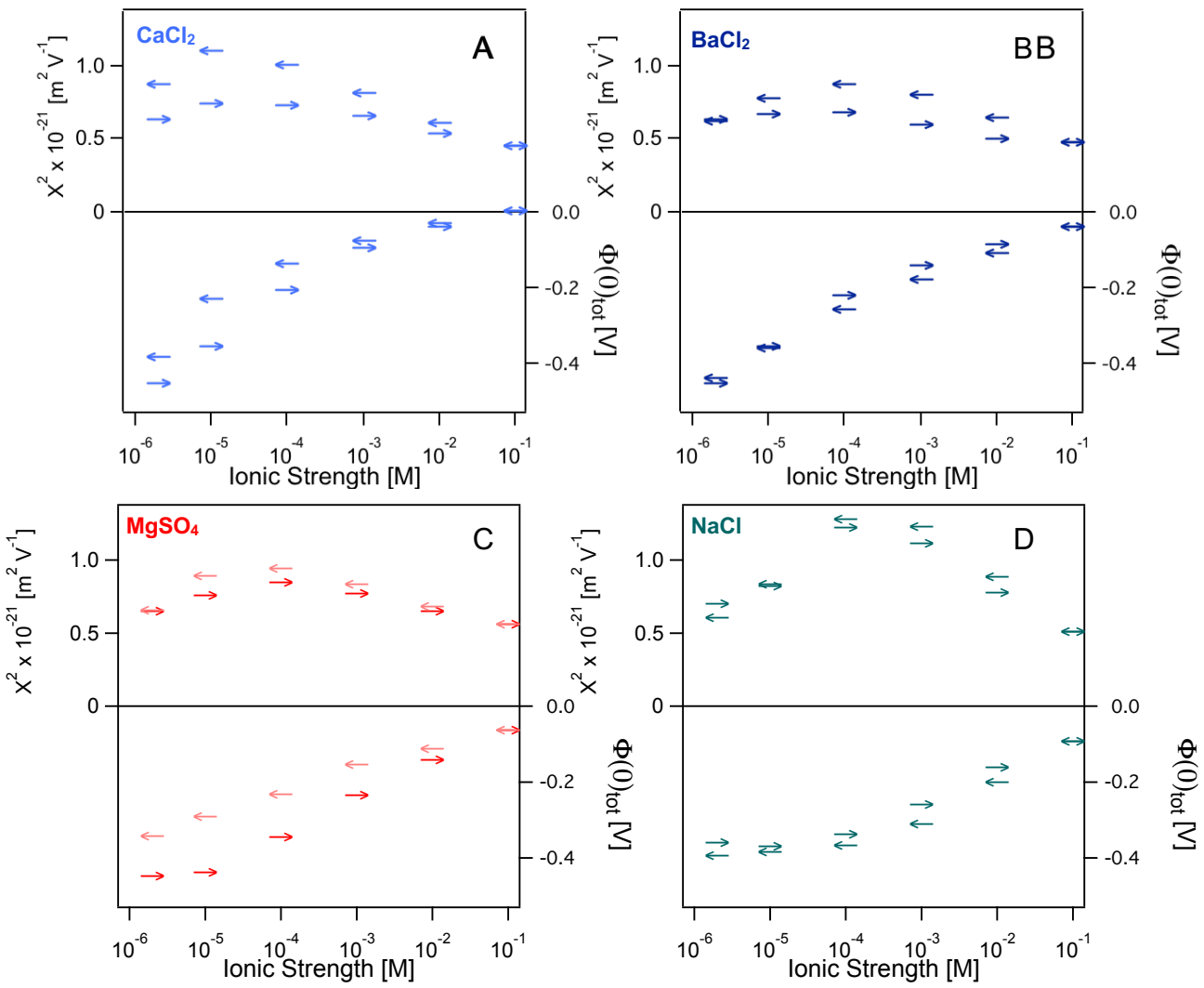
CaCl2
A
BaCl2
BB
MgSO4
C
NaCl
D
X2 x 10-21 [m2 V-1]
Φ(0)tot [V]
Ionic Strength [M]
1.0
0.5
0
0.0
-0.2
-0.4
10-6
10-5
10-4
10-3
10-2
10-1

TOC Graphic

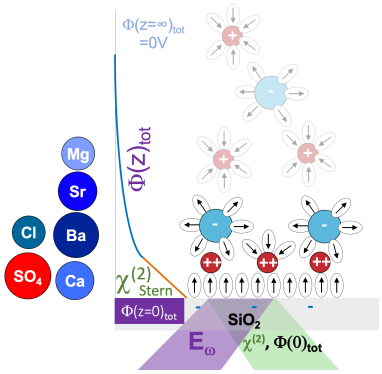
Φ(z=∞)tot
=0V
Φ(z)tot
Mg
Sr
Cl
Ba
SO4
Ca
χ(2) Stern
Φ(z=0)tot
SiO2
Eω
χ(2), Φ(0)tot